Pergamon

Int. J. Heat Mass Transfer. Vol. 39, No. 13, pp. 2771–2789, 1996

0017–9310/96 $15.00+0.00

0017–9310(95)00305–3

Heat transfer and fluid dynamics during the collision of a liquid droplet on a substrate—I. Modeling

Z. ZHAO and D. POULIKAKOS†

Mechanical Engineering Department, University of Illinois at Chicago, 842 W. Taylor Street, Chicago, IL 60680, U.S.A.

and

J. FUKAI

Chemical Engineering Department, Kyushu University, Fukuoka, 812, Japan

(*Received* 29 *November* 1994 *and in final form* 26 *July* 1995)

Abstract—This paper presents a numerical study of the fluid dynamics and heat transfer phenomena during the impingement of a liquid droplet upon a substrate. The theoretical model, based on the Lagrangian formulation, is solved numerically utilizing the finite element method. A deforming mesh is utilized to simulate accurately the large deformations, as well as the domain nonuniformity characteristic of the spreading process. The occurrence of droplet recoiling and mass accumulation around the splat periphery are standout features of the numerical simulations and yield a nonmonotonic dependence of the maximum splat radius on time. The temperature fields developing in both the liquid droplet and the substrate during the impingement process are also determined. To this end, liquid metal and water droplet collisions on different substrates were investigated. Convection effects on the temperature field development were found to be important for the entire history of spreading. These effects resulted sometimes in a practically radial temperature variation at late stages of spreading, particularly so in the cases of high impact velocities.

1. INTRODUCTION

What fluid dynamics and heat transfer phenomena occur when a liquid droplet impacts a substrate at different temperature? Scientists and engineers have been investigating various aspects of this question for more than 100 years [1, 2] because of both the inquisitive nature of science and its relevance to many engineering applications. The main motivation for the present work is in connection with the novel process of picoliter solder droplet dispensing for the mounting of microelectronic components [3] and thermal spray deposition [4, 5]. Additional applications include spray cooling of surfaces and droplet wall interaction in spray combustion.

With reference to the problem of miniature solder droplet dispension, referred to as *solder-drop-printing* technology, the shape of a solder bump produced on a micro-chip is affected by the dynamics of impact and the heat removal process from the solder droplet to the microchip substrate. The solder droplets are applied directly to the bonding pads on chips in a molten state using a similar technique as ink-on-demand for ink-jet printing [3]. With reference to thermal spray deposition, the cooling rates at the early stages of this process are extremely high (of the order of 10^6–10^8°C s^{-1}). Because of these high cooling rates, non-equilibrium states are captured by rapid solidification. The spray deposition process has been shown to produce near net shape products which eliminates the need for additional finishing steps in the manufacturing process. Moreover, the fine and homogeneous grain micro structure that appears to be resulting from the spray deposition process may eliminate the need for additional mechanical working [6–8].

Because of the aforementioned applications, the present work focuses mainly on liquid metal droplets, although water droplets are also considered. The definition of the present study is schematically shown in Fig. 1a. A molten metal droplet, originally in spherical shape, moves in the gravitational direction towards a horizontal flat substrate. The droplet velocity and diameter prior to impact are v_0 and d_0, respectively. After the droplet impacts the substrate surface, it spreads out and is flattened. In the meantime, it is cooled down by the substrate and solidifies. The present study investigates the fluid dynamics and heat transfer phenomena during the *pre-solidification* stage

† Author to whom correspondence should be addressed. Current address: Institute of Energy Technology, Swiss Federal Institute of Technology, ETH Center, Sonneggstrasse 3, CH-8092, Zurich, Switzerland.

NOMENCLATURE

c	speed of sound [m s^{-1}]
C_p	specific heat [J kg^{-1} · K^{-1}]
d_0	initial diameter of droplet [m]
Fr	Froude number
g	gravitational acceleration [m s^{-2}]
$\bar{H}$	mean surface curvature [m^{-1}]
k	thermal conductivity [W m^{-1} · K^{-1}]
M	Mach number
$\mathbf{n}$	directional cosine vector
Nu	local Nusselt number for deforming droplet
Nu_{ave}	average Nusselt number for deforming droplet
p	droplet fluid pressure [N m^{-2}]
p_0	reference pressure [N m^{-2}]
Pr	Prantdl number
Pe	Peclet number
q	heat flux [W m^{-2}]
Q_w	splat/substrate interface heat flux [W m^{-2}]
r	radial coordinate [m]
r_0	initial radius of droplet [m]
R_{max}	dimensionless maximum radius of splat
$R_c(\tau)$	dimensionless radius of the droplet/substrate contact circle
Re	Reynolds number
s	coordinate measured along the free surface of the deforming droplet [m]
t	time [s]
T	temperature [K]
T_0	droplet initial temperature [K]
T_w	substrate initial temperature [K]
u	radial direction velocity [m s^{-1}]
v	axial direction velocity [m s^{-1}]
v_0	droplet impact velocity [m s^{-1}]
We	Weber number
x	radial coordinate [m]
z	axial coordinate [m].

Greek Symbols

α	thermal diffusivity [m^2 s^{-1}]
γ	surface tension coefficient [N m^{-1}]
η	dimensionless thermal penetration depth
θ	azimuthal coordinate
Θ	dimensionless temperature
μ	viscosity [kg s · m^{-1}]
ν	kinematic viscosity [m^2 s^{-1}]
σ	stress [N m^{-2}]
τ	dimensionless time.

Subscripts

r	radial direction
w	substrate
z	axial direction
0	initial
1	droplet
2	substrate.

of the impact process. Solidification will constitute the focus of future work.

The heat and fluid flow phenomena occurring during the impact of a single liquid-metal droplet on a cold substrate are not conventional or easy to study. There are several reasons for this fact: the fluid dynamics of the droplet spreading is a free surface problem with large domain deformations in the presence of surface tension, and with possible droplet break-up phenomena and three-dimensional effects. Contact line issues have to be resolved in the numerical model. The heat transfer process involves convection and steep temperature gradients within a severely deforming domain, coupled with conduction in the substrate. A review of the existing relevant (mainly theoretical and numerical) literature is outlined in the following paragraphs.

Numerical efforts targeting the fluid dynamics of the droplet impingement process initially adopted oversimplifying assumptions in order to facilitate the solution. To this end, Harlow and Shannon [11] neglected both viscous and surface-tension effects in their modeling formulation of a liquid droplet impacting on a flat plate. The 'market in cell' (MAC) technique [12–14] based on a fixed grid was employed in the above work which pioneered the simulation efforts of the splashing process. Subsequent models [10] involved simplified treatments of the fluid spreading process, but incorporated provisions for phase change. Madejski [15, 16] circumvented the difficulties (as well as the benefits) associated with the knowledge of the fluid mechanics of the droplet spreading by simply considering an order of magnitude balance between the inertial, viscous, and surface-tension effects of the splashing process, and reported on the asymptotic values of the degree of spreading of liquid-metal droplets impacting on horizontal and inclined plates. A numerical model presented recently by Trapaga and Szekely [17], gave a detailed characterization of the droplet deformation process on a solid plate, treating the free-surface deformation through a combination of the MAC and 'volume of fluid' (VOF) methods. The employment of a fixed grid could not be avoided since Trapaga and Szekely [17] utilized the commercially available FLOW3D code [18] to carry out their numerical simulations. Since the spreading process involves large deformations (for example, the splat thickness is commonly 20 times smaller than the

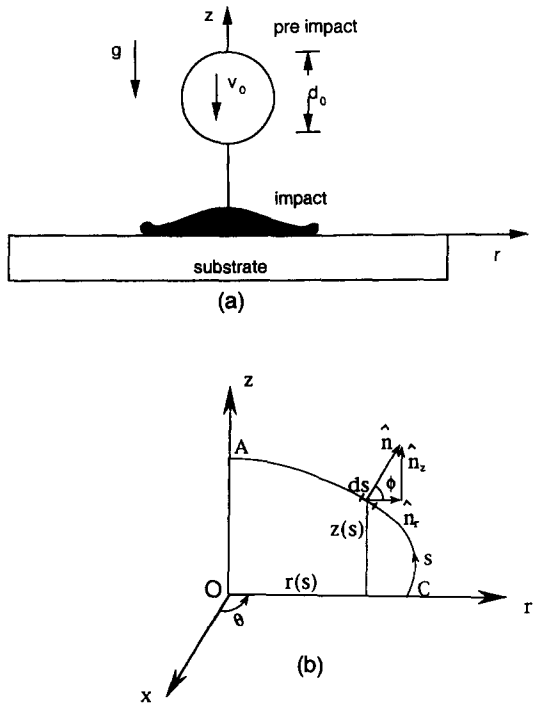

Fig. 1. (a) Schematic of the problem of interest. (b) Schematic defining the coordinate system in the deforming droplet.

initial droplet diameter), as well as severe non-uniformities across the splat thickness occurring during spreading, the employment of a fixed grid may be questionable. This also applies at late times of the process when the heat transport takes place. Finite difference simulations of droplet spreading on a flat surface based on MAC and SOLA-VOF [19] methods with fixed grids were also used by Tsurutani *et al.* [20], Watanabe *et al.* [21], and Pasandideh-Ford and Mostaghimi [22].

Fukai *et al.* [23] presented a finite element technique to model the droplet spreading process. This technique accounted for the presence of inertial, viscous, gravitational and surface tension effects. In contrast to other earlier studies of the droplet impingement process, mentioned above, the Lagrangian approach was employed because it facilitates the accurate simulation of the motion of the deforming free surface. As a result, the formation of a propagating ring structure (due to mass accumulation) at the periphery of the splat, as well as recoiling and subsequent oscillation of the splat were predicted by the numerical simulations. For the modeling of the splashing fluid dynamics, the present study relies on the recent work of Fukai *et al.* [23]. This model and the associated numerical methodologies are extended to account for the relevant convection and conduction heat transfer phenomena both in the droplet and the substrate.

2. THE MATHEMATICAL MODEL

(*a*) *Fluid dynamics*

The model is formulated to simulate the impact of a liquid droplet on a substrate, starting at the instant that the droplet comes into contact with the substrate and proceeding until the droplet comes to rest after the splashing process is completed [23]. The Lagrangian approach is adopted because it facilitates the accurate simulation of the motion of the deforming free surface [23, 24]. In the following dimensionless axisymmetric conversation equations within an initially spherical droplet impaction on a solid surface, r, z and θ are, the radial, axial, and azimuthal coordinates respectively, (Fig. 1b), ρ is the fluid density, u the radial velocity component, v the axial velocity component, t the time, p the pressure, μ the viscosity, v the kinematic viscosity, g the gravitational acceleration, c the speed of sound in the fluid medium, and γ the surface tension.

The stresses tensor components are denoted by σ_{ij}.

$$\frac{\partial P}{\partial \tau}+\frac{1}{M^2}\left(\frac{1}{R}\frac{\partial}{\partial R}(RU)+\frac{\partial V}{\partial Z}\right)=0 \tag{1}$$

$$\frac{\partial U}{\partial \tau}-\frac{1}{R}\frac{\partial}{\partial R}(R\bar{\sigma}_{rr})-\frac{\partial \bar{\sigma}_{rz}}{\partial Z}+\frac{\bar{\sigma}_{\theta\theta}}{R}=0 \tag{2}$$

$$\frac{\partial V}{\partial \tau}-\frac{1}{R}\frac{\partial}{\partial R}(R\bar{\sigma}_{rz})-\frac{\partial \bar{\sigma}_{zz}}{\partial Z}-\frac{1}{Fr}=0. \tag{3}$$

The dimensionless initial and boundary conditions of the problem are [23, 25]

$$\begin{aligned}&\tau=0: \quad U=0, \quad V=-1, \quad P=\frac{2}{We}\\ &R=0: \quad U=0, \quad \frac{\partial V}{\partial R}=0,\\ &Z=0: \quad U=V=0.\end{aligned} \tag{4}$$

At the surface,

$$\bar{\sigma}_{rr}n_r+\bar{\sigma}_{rz}n_z=-2\frac{\bar{H}}{We}n_r \tag{5}$$

$$\bar{\sigma}_{rz}n_r+\bar{\sigma}_{zz}n_z=-2\frac{\bar{H}}{We}n_z. \tag{6}$$

The nondimensionalization was carried out according to the following definitions:

$$\begin{aligned}&R=\frac{r}{r_0}, \quad Z=\frac{z}{r_0}, \quad S=\frac{s}{r_0}, \quad \bar{H}=\frac{H}{1/r_0}\\ &\tau=\frac{t}{r_0/v_0}, \quad U=\frac{u}{v_0}, \quad V=\frac{v}{v_0}, \quad P=\frac{p-p_0}{\rho v_0^2}\\ &\bar{\sigma}_{ij}=\frac{\sigma_{ij}+\delta_{ij}p_0}{\rho v_0^2},\end{aligned} \tag{7}$$

where δ_{ij} is the Kroneker delter and the mean curvature of the free surface is defined as

$$\bar{H} = \frac{r^2(r'z'' - z'r'') + [(r')^2 + (z')^2]rz'}{2r^2[(r')^2 + (z')^2]^{3/2}}. \quad (8)$$

The primes denote differentiation with respect to s (Fig. 1b). The nondimensionalization process created the following dimensionless groups (Reynolds, Weber, Froude and Mach numbers respectively):

$$Re = \frac{v_0 r_0}{\nu} \quad We = \frac{\rho r_0 v_0^2}{\gamma} \quad Fr = \frac{v_0^2}{r_0 g} \quad M = \frac{v_0}{c}. \quad (9)$$

Note that the time derivative has been maintained in the continuity equation to facilitate the numerical solution of the model, as explained in detail in refs. [23, 25]. At this point the mathematical model for the fluid dynamics of the droplet impact process is complete.

(b) Heat transfer

The Lagrangian formulation is used to construct the mathematical model for the conjugate heat transfer process in the droplet and the substrate (Fig 1a). The relevant energy conservation equations, initial and matching conditions are:

Energy equation in the splat

$$\frac{\partial \Theta_1}{\partial \tau} = \frac{1}{Pe_1}\left[\frac{1}{R}\frac{\partial}{\partial R}\left(R\frac{\partial \Theta_1}{\partial R}\right) + \frac{\partial^2 \Theta_1}{\partial Z^2}\right]. \quad (10)$$

Energy equation in the substrate

$$\frac{\partial \Theta_2}{\partial \tau} = \frac{1}{Pe_2}\left[\frac{1}{R}\frac{\partial}{\partial R}\left(R\frac{\partial \Theta_2}{\partial R}\right) + \frac{\partial^2 \Theta_2}{\partial Z^2}\right]. \quad (11)$$

Initial conditions

$$\tau = 0: \quad \Theta_1(R, Z, 0) = 1 \quad \Theta_2(R, Z, 0) = 0. \quad (12)$$

Boundary conditions at the droplet free surface and the substrate boundary surface:

$$\frac{\partial \Theta_i}{\partial R} n_r + \frac{\partial \Theta_i}{\partial Z} n_z = 0 \quad i = 1, 2. \quad (13)$$

Splat/Substrate interface condition

$$\Theta_1 = \Theta_2 \quad -k_1 \frac{\partial \Theta_1}{\partial Z} = -k_2 \frac{\partial \Theta_2}{\partial Z}. \quad (14)$$

In the substrate far from the interface

$$\Theta_2(R, -\infty, \tau) = \Theta_2(\infty, Z, \tau) = 0. \quad (15)$$

The nondimensionalization was carried out according to the following definitions:

$$\Theta_i = \frac{T_i - \min(T_0, T_w)}{|T_0 - T_w|}, \quad i = 1, 2. \quad (16)$$

The nondimensional groups in the energy equations are the Peclet numbers for the splat and the substrate

$$Pe_1 = \frac{r_0 v_0}{\alpha_1} \quad Pe_2 = \frac{r_0 v_0}{\alpha_2}. \quad (17)$$

In the above equations T, T_0 and T_w are the temperature, the droplet initial temperature, and the substrate initial temperature; k is the thermal conductivity and α the thermal diffusivity. The subscripts 1, and 2 stand for droplet and substrate, respectively. The remaining quantities were defined earlier in connection with the fluid dynamics model. Note that the energy equations in the fluid and the substrate have exactly the same form in the Lagrangian formulation. Therefore, the fluid region can be combined with the solid region and the energy equations can be solved in this combined region following the same numerical procedure. The convective effect on the transfer of energy in the splat is implicit in the Lagrangian formulation. This convective effect is represented by the movement of fluid particles in the deforming droplet.

3. NUMERICAL SOLUTION PROCEDURE

The mathematical model outlined in the previous section was solved numerically by invoking the finite element method. To solve the problem numerically, the artificial compressibility method [26–28] was utilized, as has become apparent by the mathematical formulation of the previous section. An important advantage of this method is that it provides a pressure evolution equation. The main premise of this method is that it assumes a 'slight' compressibility to exist in flows that are essentially incompressible, like the liquid flow under investigation. According to the artificial compressibility method, the speed of sound in 'real' incompressible fluids is assumed to be very large, but not infinite. This allows for the casting of the continuity equation in the form shown earlier, equation (1). Note that as the Mach number in equation (1) approaches zero (the speed of sound approaches infinity), the continuity equation reduces to the conventional form used in incompressible flow modeling. The presence of the pressure derivative in equation (1) allows for the explicit integration of all the conservation equations in time.

The Galerkin method was utilized for the solution of the numerical model. An implicit method was employed for the numerical integration in time. Since the obtained algebraic equations are strongly nonlinear in space, an iterative procedure at each instant in time was necessary. To this end, the technique proposed by Bach and Hassager [23, 24] was utilized. For the solution of the energy equations, the substrate mesh was generated and coupled with the droplet mesh. The energy equations for splat and substrate were solved on the combined mesh of the splat and substrate.

As the splashing process advanced in time, the distortion of the finite elements became exceedingly large. To circumvent this difficulty, a criterion was introduced according to which a new triangular finite

element grid was generated when the distortion of the existing grid exceeded a threshold value. This criterion is expressed by

$$(L_b - L_h)/(L_b - L_h)_{ref} \leqslant 4, \tag{18}$$

where L_b represents the longest side (base) of a triangular element, L_h the corresponding triangle height, and the subscript 'ref' denotes a reference value at the time the element was generated. The procedure for the droplet mesh generation and remeshing is the same as in ref. [23] and shall not be presented here. Additional details can be found in ref. [25].

The substrate mesh is generated using the droplet element nodes on the splat/substrate interface as a guide at each time step. The dimension of the substrate increases with time according to the growth of the thermally affected area. An estimate of the thickness of this area is obtained from the thermal boundary layer thickness in an semi-infinite wall subjected to a constant surface temperature that is higher than its initial temperature. It can be shown [29] that the dimensionless thermal penetration depth in this case ($\eta = z/r_0$) is proportional to $2\sqrt{(\tau/Pe_2)}$. This relation was used as the growth function of the axial dimension of the substrate computational domain. The radial dimension of the substrate computational domain increases as the droplet spreads. Both substrate dimensions were controlled such that they either grew or stayed unchanged with the advancement of time. They were never allowed to shrink during the droplet recoiling. In all cases increasing the substrate dimensions further left the results unchanged: The substrate was modelled as a semi-infinite body.

The resulting algebraic equations from the Galerkin finite element discretization of the fluid dynamics equations are non-symmetric. The discretized energy equations are symmetric. A full-bandwidth solver is used for the discretized fluid dynamics equations in the droplet domain and a half-bandwidth solver for the discretized energy equations on the combined splat and substrate mesh. To this end, the Cuthill–McKee algorithm [30] is applied to minimize equation bandwidth for the splat mesh in the fluid dynamics calculation and for the combined splat and substrate mesh in the heat transfer calculation, respectively.

An important issue in the numerical calculation is related to the boundary condition at the liquid–solid interface. The relation between contact angle and lateral velocity of the liquid–solid contact line has been extensively analyzed in the limit of slow motion using such mathematical techniques as the perturbation method and the collocation method. Haley and Miksis [31] investigated the above problem for situations where the capillary force, which acts at the contact line, dominates the droplet spreading motion. They used four types of mathematical models which included the dynamic and/or static contact angle, as well as other parameters concerned with the slip condition at a liquid–solid interface. A general mathematical model capable of describing the motion of the contact line has not been yet identified.

It is established that the traditional no-slip boundary condition fails in the vicinity of the contact line [32–34]. This line separates a fluid interface from a solid surface, and is characterized by an infinite stress if the no-slip condition is enforced on it. In order to circumvent this problem, different slip models have been postulated to describe the macroscopic flow behavior of the contact line motion. The most popular one is the Navier slip model discussed in detail by Dussan [34], and Silliman and Scriven [35]. The spreading motion of a fluid has been simplified by neglecting the inertial and gravitational effects, so that the lubrication approximation or matched asymptotic expansions could be employed [36–38]. Fukai *et al.* modeled the effect of surface wetting on the droplet splashing process [39]. The contact angle hysteresis between advancing and receding motions of the contact line was accounted by using constant dynamic contact angles for the advancing and receding motions of the contact line, respectively. The advancing and receding contact angles were measured *a priori* experimentally.

According to Bach and Hassager [24] two separate boundary conditions need to be prescribed at each boundary node on a slip surface: one velocity and one force condition. The contact point C shown in Fig. 1b, which lies on the slip line separating the droplet free surface (AC) from the no-slip solid/liquid interface (OC), is characterized by $v = 0$ (no penetration) and the force boundary condition expressed by equation (5). The same is true for all points on the contact (slip) line. Our formulation, following ref. [24], does not force the contact angle to assume a specific value. It merely imposes a net interfacial force at the contact line. The assumption is made that this interfacial force is given by the equilibrium surface-tension coefficients of the joining phases during flow. This level of physical modeling is consistent with the assumptions inherent in equation (5) with a constant coefficient of surface tension, γ.

When a point of the free surface contacts the substrate for the first time, a temperature value needs to be assigned to this new contact point before solving the energy equation for the combined physical domain of splat and substrate. To this end, a local enthalpy balance is applied in the neighbourhood of this contact point to obtain its temperature. A local enthalpy balance requires that the summation of element enthalpies, for the elements connected to a contact point (C, Fig. 1b) remains unchanged right before and right after this point attaches onto the substrate surface [25].

In order to illustrate the ability of the numerical model presented in the previous sections to produce physically acceptable solutions, a wide array of calculations were performed involving a variety of process parameters. The time step and numerical grid insensitivity of the model predictions were examined

for both the fluid dynamics and the heat transfer aspects of the process at the initial stages of this study. The test results for the time step size and the mesh grid size are not shown herein due to space limitations. They are presented in detail in ref. [25]. We found that the number of finite elements needed for time-step and grid independent results varied according to the final degree of deformation of a droplet. Typically, approximately 5000 finite elements were necessary for the droplet along with a time step $\Delta\tau$ in the range of 10^{-3}–10^{-4} and 1000 to 10 000 elements were necessary for the substrate, depending on the thermal diffusivity of the substrate material. The intensive computations were performed on a DEC 5000PXG workstation and a Cray Y-MP supercomputer.

4. RESULTS AND DISCUSSION

The numerical simulations examined the effects of the substrate material, impact velocity, and droplet Prandtl number on the cooling of molten metal and water droplets. The overall (contact area averaged) Nusselt number at the substrate surface is also reported for a host of conditions. This Nusselt numbers is defined as follows:

$$\overline{Nu}(R,\tau)=\frac{\int_0^{R_c(\tau)}2\pi RNu(R,\tau)\mathrm{d}R}{\int_0^{R_c(\tau)}2\pi R\mathrm{d}R}, \tag{19}$$

where

$$Nu(R,\tau)=\frac{Q_w(R,\tau)}{\Theta_w(R,\tau)-\Theta_0} \tag{20}$$

$$Q_w(R,\tau)=-\left.\frac{\partial\Theta_1(R,Z,\tau)}{\partial Z}\right|_{z=0} \tag{21}$$

are the local Nusselt number and the dimensionless local heat flux across this interface, respectively, and $\Theta_w(R,\tau)$, $R_c(\tau)$ are the dimensionless interface temperature and dimensionless radius of the droplet/substrate interface circle.

Effect of substrate material on the cooling of a liquid metal droplet

The first set of simulations examines the effect of the substrate material on the cooling of a molten metal droplet in low speed spray coating or high speed solder deposition applications. The temperature distribution is represented by the contour lines denoting the isotherms (Fig. 2). The instantaneous stream lines and velocity vectors are also plotted in the left half of the droplet region for the better illustration of fluid flow effects on the thermal development history of the droplet. A tin droplet of radius $r_0 = 9\mu$m was considered to impinge on three different substrates at a velocity $v_0 = 29.4\ \mathrm{m\,s^{-1}}$. For molten tin, the following property values were used: surface-tension coefficient $\gamma = 0.544\ \mathrm{N\,m^{-1}}$, density $\rho = 7000\ \mathrm{kg\,m^{-3}}$, kinematic viscosity $\nu = 2.64\times10^{-7}\ \mathrm{m^2\,s^{-1}}$, thermal diffusivity $\alpha = 1.714\times10^{-5}\ \mathrm{m^2\,s^{-1}}$, and thermal conductivity $k = 30\ \mathrm{W\,m^{-1}\cdot K^{-1}}$. The values of the relevant dimensionless groups are $Re = 1000$, $We = 100$, $Fr = 10^7$. The substrate materials examined are copper, steel and glass, respectively, to cover a large portion of the spectrum of the thermal diffusivity and the thermal conductivity. The thermal diffusivity and thermal conductivities for the substrate materials used in the simulations are correspondingly $1.17\times10^{-4}\ \mathrm{m^2\,s^{-1}}$ and $401\ \mathrm{W\,m^{-1}\cdot K^{-1}}$ for copper, $3.95\times10^{-6}\ \mathrm{m^2\,s^{-1}}$ and $14.9\ \mathrm{W\,m^{-1}\cdot K^{-1}}$ for steel (AISI 304 stainless steel), and $7.47\times10^{-7}\ \mathrm{m^2\,s^{-1}}$ and $1.4\ \mathrm{W\,m^{-1}\cdot K^{-1}}$ for glass.

It is immediately apparent from Fig. 2a–c that the cooling of the impinging droplets occurs simultaneously with the spreading. In the entire droplet spreading process the droplet temperature field demonstrates convective and two-dimensional features. In all cases, the fluid temperature is higher in the center region and lower around the spreading front. This is because high temperature fluid is continuously supplied to the center region, and the splat periphery is continuously cooled down by contacting the low temperature surface of the substrate as it spreads outward. In the cases of steel and glass substrates, at late stages of the droplet spreading ($\tau = 4.0$, Fig. 2c), the temperature distribution within the splat is largely one-dimensional. The temperature gradients within the splat occur in the radial, rather than the axial, direction despite the fact that the splat thickness is much smaller than the splat diameter. It appears that at this time the center of the splat is cooled by the splat periphery rather than the substrate. This is a result of the strongly convective nature of the cooling process at the earlier stages and implies that approximate modeling attempts using an axial heat conduction model for a thin disk to simulate the heat transfer within the fully spread droplet, are not accurate when the thermal conductivity of the substrate is low. The premise that 'the droplet spreads first and cools down later' associated with the early analyses of splat cooling and thermal spray deposition may not be always valid.

As shown in Fig. 2a–c, the copper substrate temperature changes very little during the entire process of spreading, while the glass substrate temperature increases rapidly in the neighborhood of the splat/substrate interface. The droplet impacting on the copper substrate cools down the fastest compared to the droplets impacting on the steel and glass substrates under identical conditions. The flow structure is dominated by the inertial force at the intial stages of spreading. The flow structure experiences a drastic change at the late stages of spreading when the inertial force decreases as the fluid spreading slows down by the action of surface tension forces. Noteworthy is the mass accumulation around the periphery of the splat. A secondary flow vortex emerges near the contact line (magnified in the detail of Fig. 2c). The vortex grows

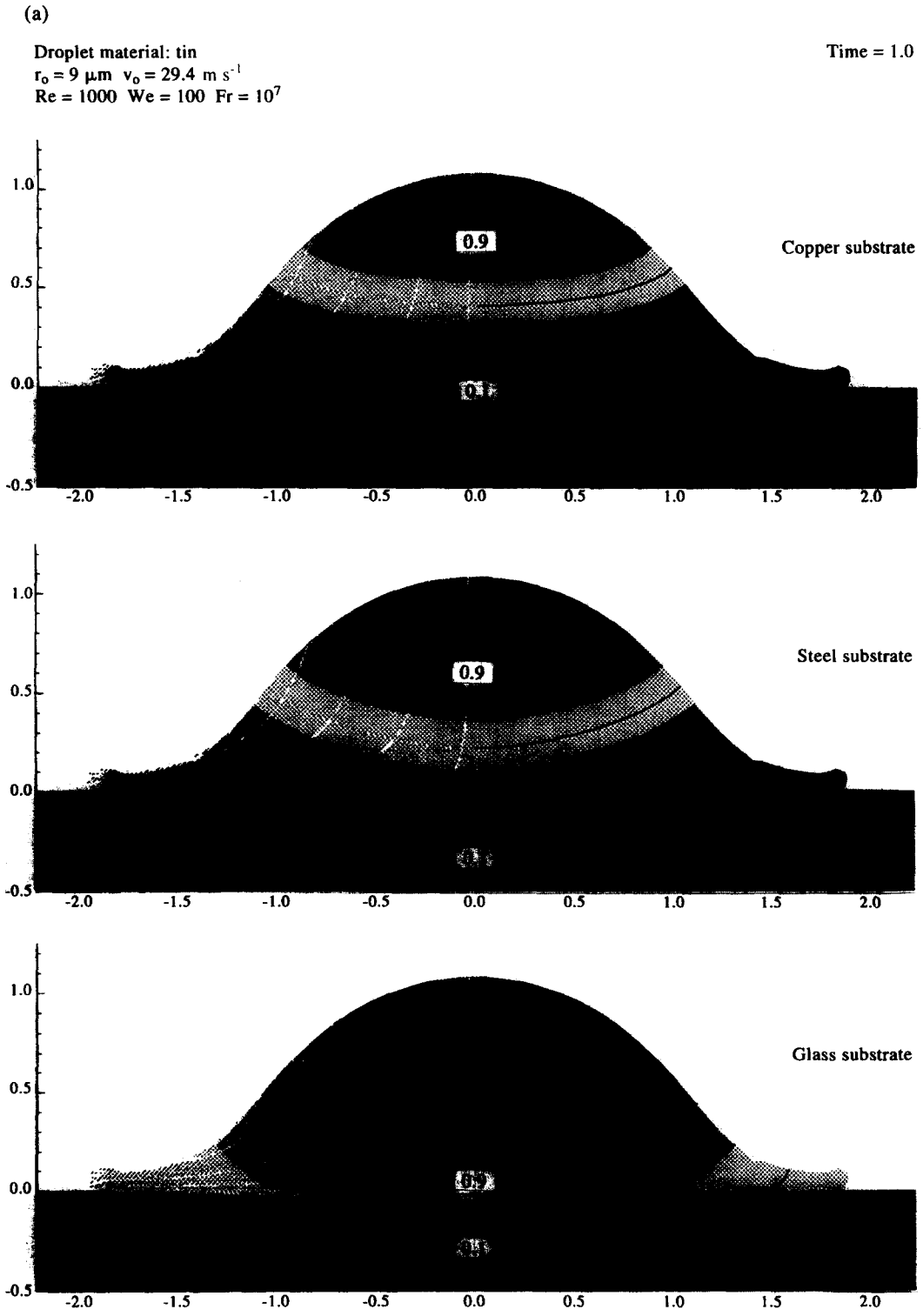

Fig. 2. Tin droplet spreading on different substrates: (a) $\tau = 1.0$, (b) $\tau = 2.0$, (c) $\tau = 4.0$. (*Continued overleaf.*)

(b)

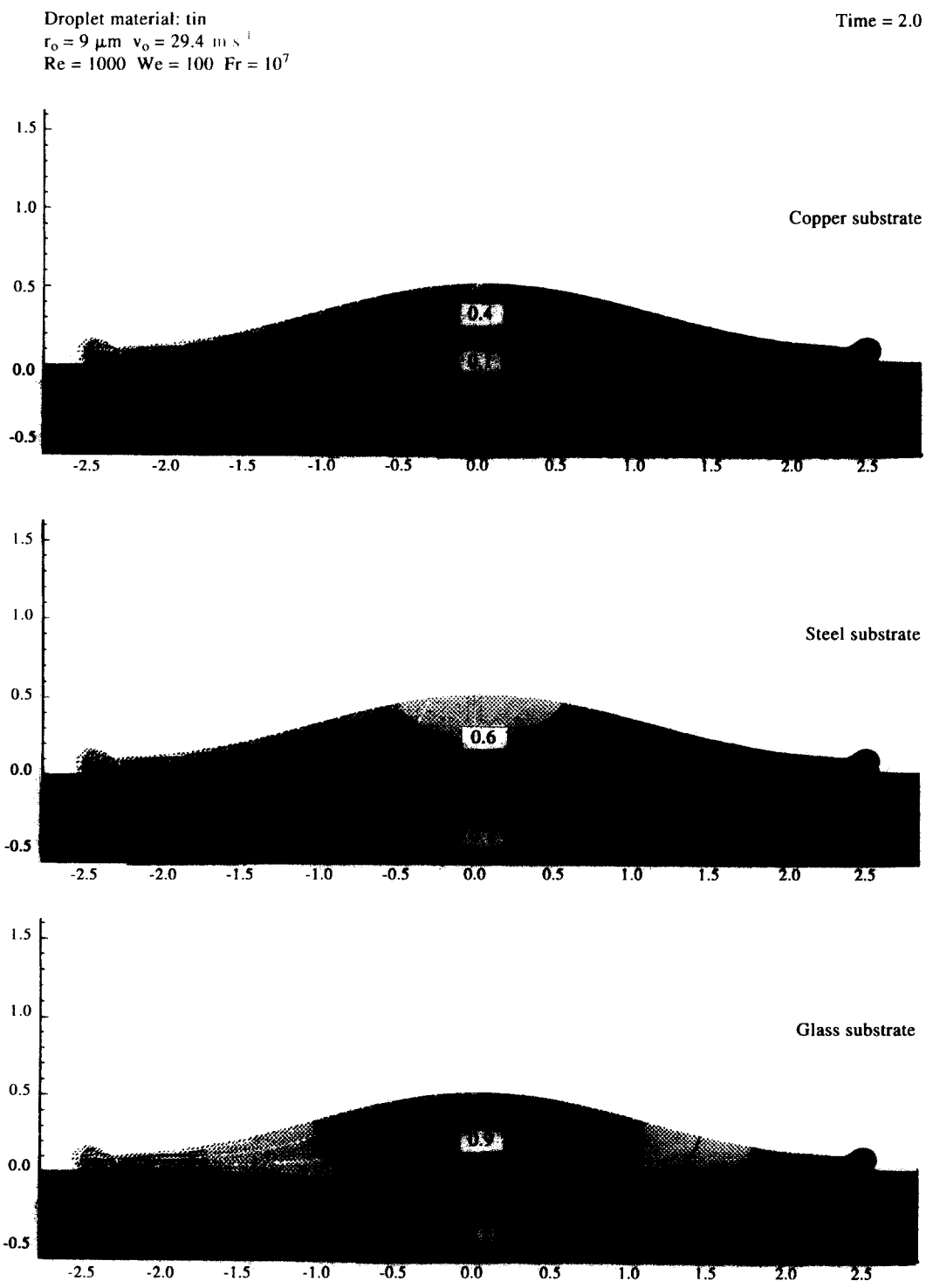

Fig. 2—*continued.*

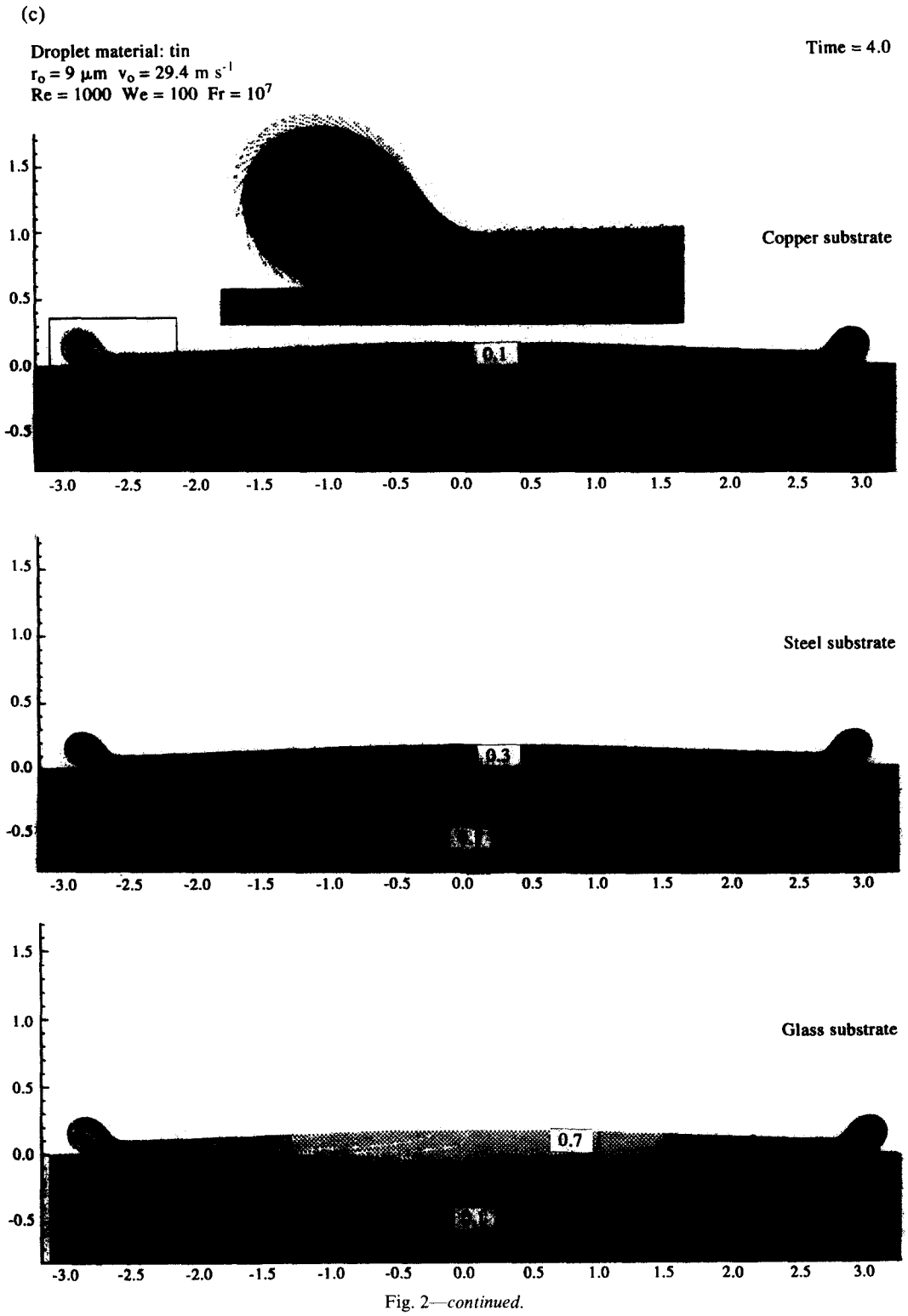

Fig. 2—*continued.*

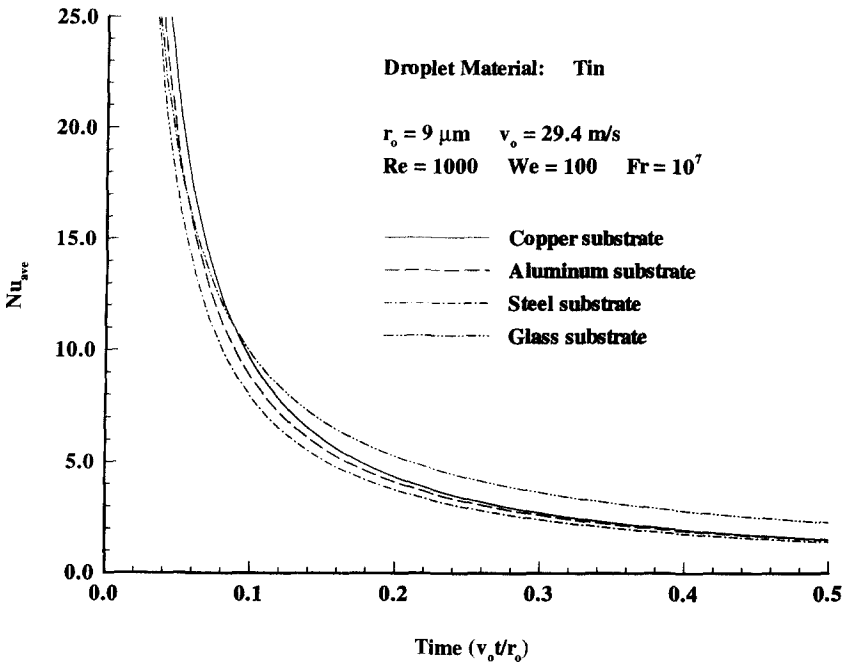

Fig. 3. Variation of the average Nusselt number with time for a host of substrate materials.

larger and moves up to the top of the free surface in the splat periphery region.

The average temporal Nusselt numbers for four different substrates are shown in Fig. 3. It is immediately apparent that the Nusselet number decreases rapidly during the initial stage of impact and approaches a plateau value late in the spreading process. The Nusselt number is higher for the more conductive substrates compared to the less conductive substrates at the initial stage of impact. It is interesting to note that the Nusselt number for the glass substrate surpasses that of the more conductive metal substrates at later times ($\tau > 0.1$). This result is due to the fact that the Nusselt number is determined by two competing quantities, i.e. the heat flux across the interface and the difference between the wall temperature and the reference temperature [equations (18)–(20)]. Detailed examination of each competing quantity [25] (not shown here for brevity) showed that while the heat flux across the interface, Q_w, is much higher for the case of the copper substrate compared to the glass substrate, the temperature difference, $\Theta_w(R,\tau)-\Theta_0$, is also much higher for the case of copper substrate. The aggregate effect of interface heat flux and wall temperature difference resulted in a lower Nusselt number for the copper substrate at later times.

Cooling of different hot substrates by a water droplet

This set of numerical simulations aimed at a detailed examination of the temperature field, developing under a substrate surface cooled by an impacting water droplet. The simulation conditions were chosen for typical spray cooling applications. A water droplet of radius $r_0 = 0.345$ mm was considered to impinge on an aluminum and a glass substrate at a velocity $v_0 = 1.46\ \mathrm{m\,s^{-1}}$. The following physical property values were used for water in the numerical simulations: surface-tension coefficient $\gamma = 0.073\ \mathrm{N\,m^{-1}}$, density $\rho = 1000\ \mathrm{kg\,m^{-3}}$, kinematic viscosity $\nu = 10^{-6}\ \mathrm{m^2\,s^{-1}}$ thermal diffusivity $\alpha = 1.428 \times 10^{-7}\ \mathrm{m^2\,s^{-1}}$, and thermal conductivity $k = 0.598\ \mathrm{W\,m^{-1}\cdot K^{-2}}$. The above conditions resulted in the following relevant droplet dimensionless numbers: $Re = 500$, $We = 10$, $Fr = 630$ and $Pr = 7$.

Figure 4a–c depicts a sequence of frames corresponding to different instances of the substrate cooling process. A different palette is used in order to reveal more details of the substrate temperature contours. The isotherms are equally spaced, but on different scales for the glass substrate and the aluminum substrate, respectively, in order to effectively visualize the temperature fields in the substrate region. The temperature scale range for glass and aluminum substrate cases are 0.095–0.995 and 0.9–1, respectively. The spray cooling sequences shown in Fig 4a–c reveals the significant differences between the glass and the aluminum substrates. Like the earlier case of a molten tin droplet impacting on different substrates, the conductive (aluminum) substrate temperature changes very little during the entire water droplet cooling process. On the other hand, the glass substrate temperature is noticeably reduced in the region immediately under the splat. By comparing the contour lines with the dimensionless temperature value of 0.995 in both the glass and the aluminum substrates, it can be seen that the cooling effect of the splashing water droplet penetrates almost twice as deep into the aluminum substrate than the glass substrate. From

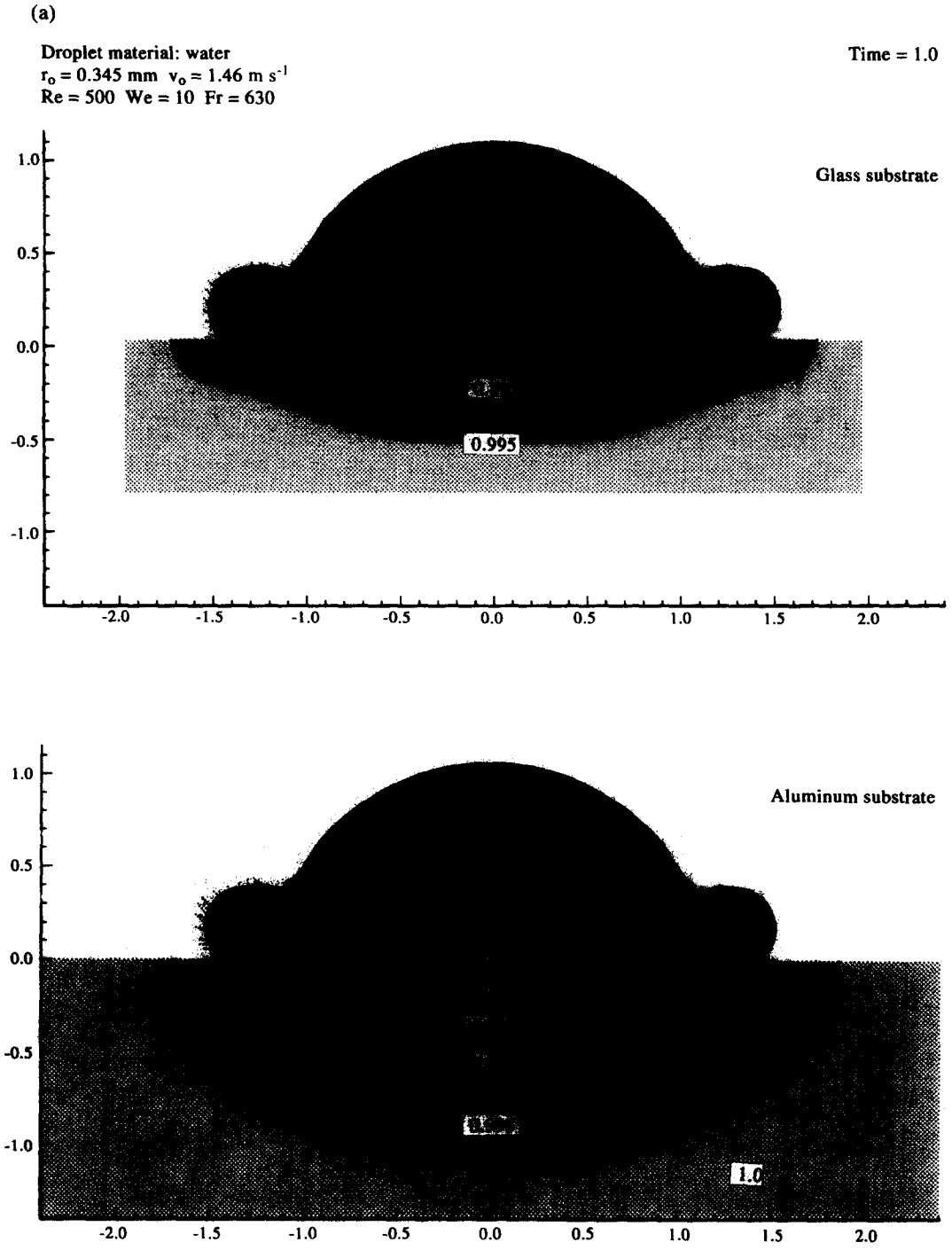

Fig. 4. Water droplet spreading on different substrates: (a) $\tau = 1.0$, (b) $\tau = 2.0$, (c) $\tau = 4.0$. (*Continued overleaf.*)

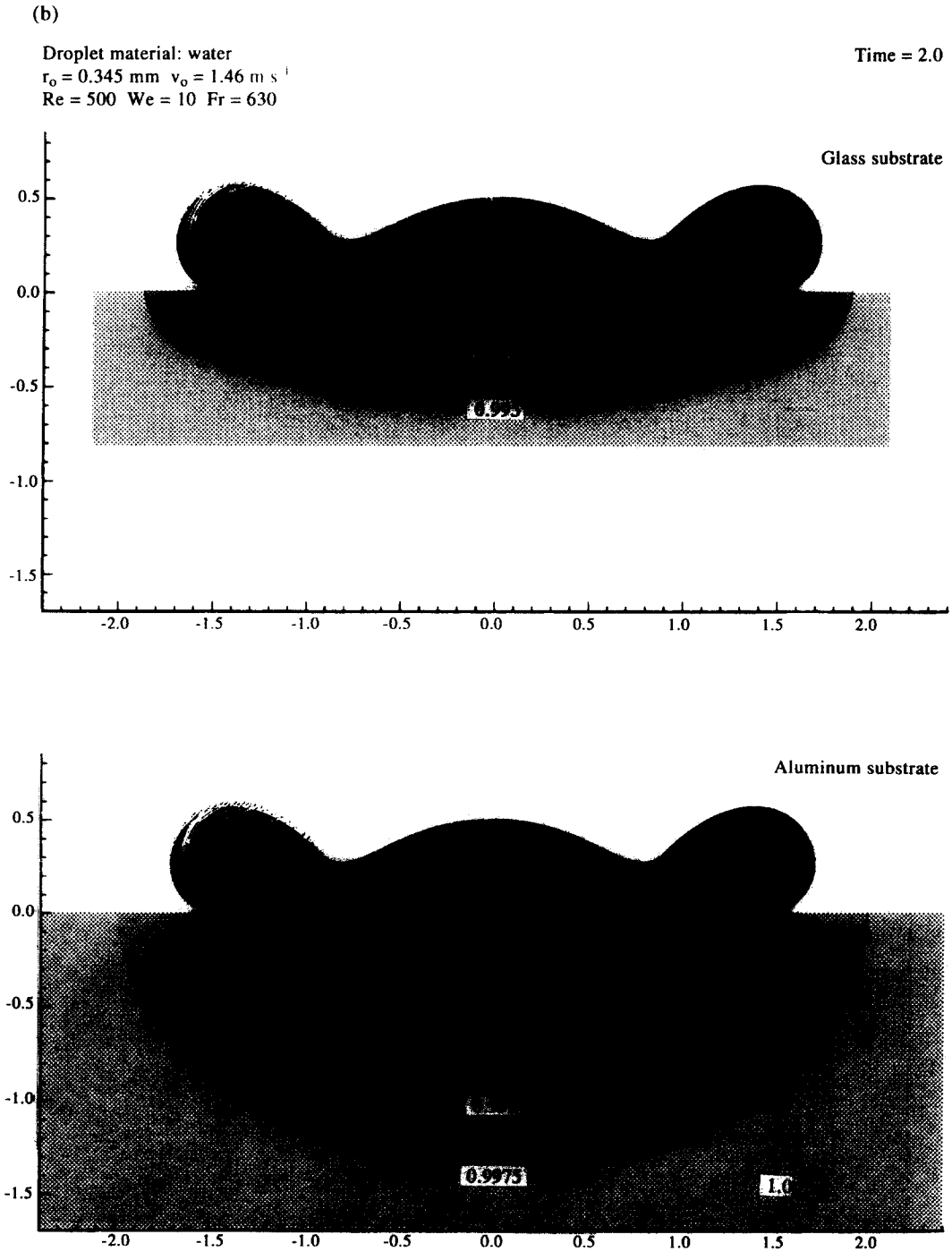

Fig. 4 —*continued.*

(c)

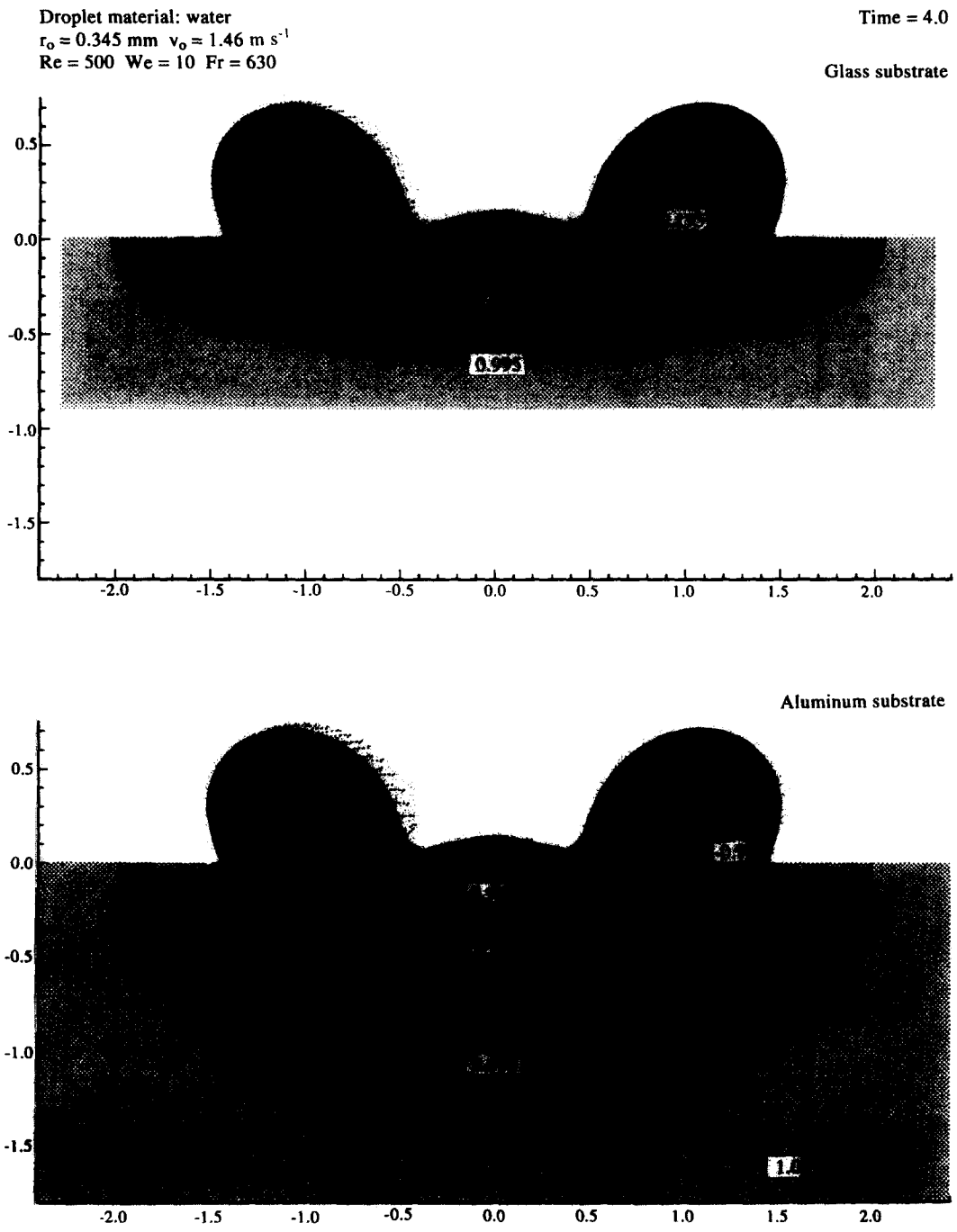

Fig. 4—*continued.*

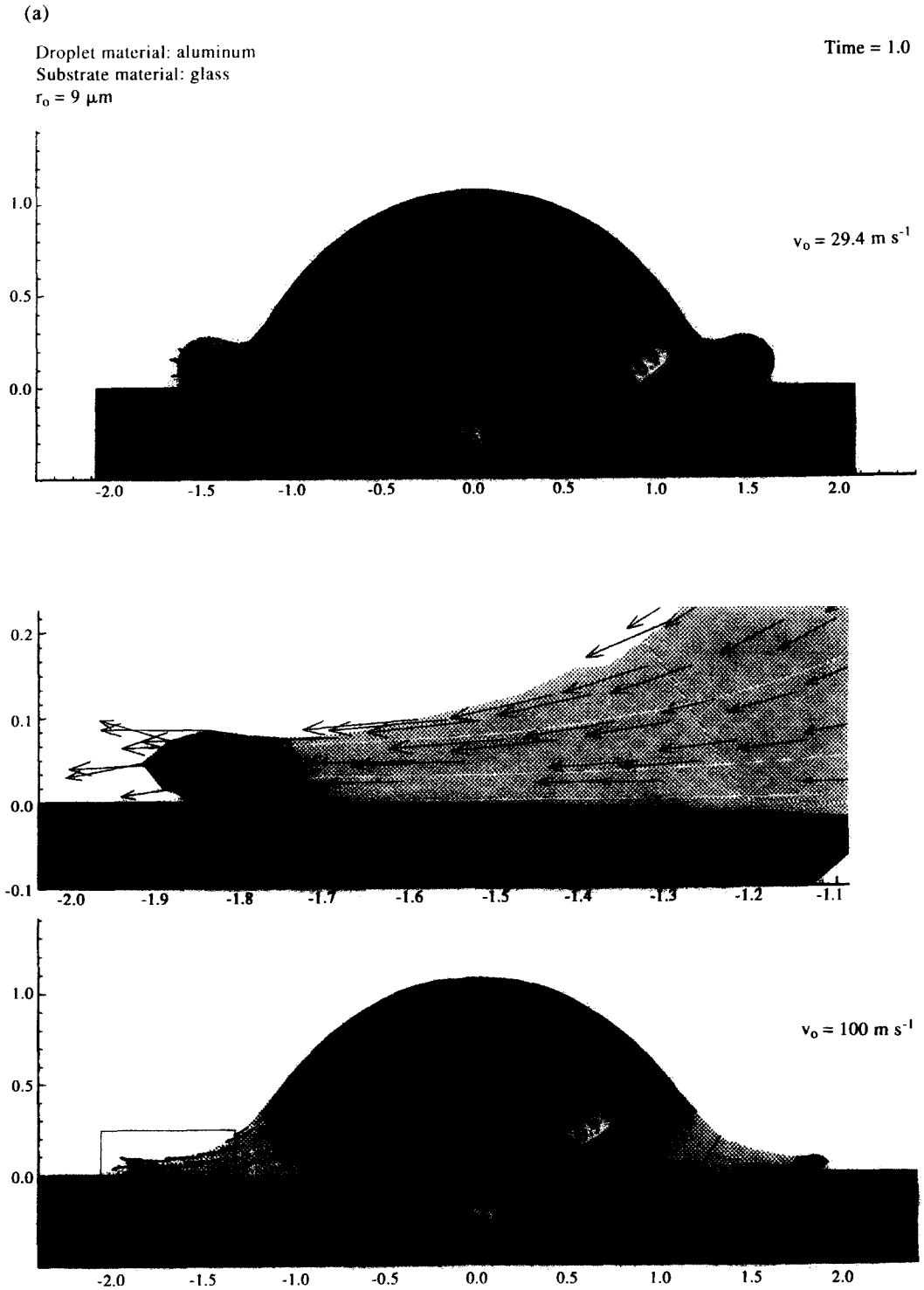

Fig. 5. Aluminum droplet spreading on a glass substrate at different impact velocities: (a) $\tau = 1.0$, (b) $\tau = 2.0$, (c) $\tau = 4.0$.

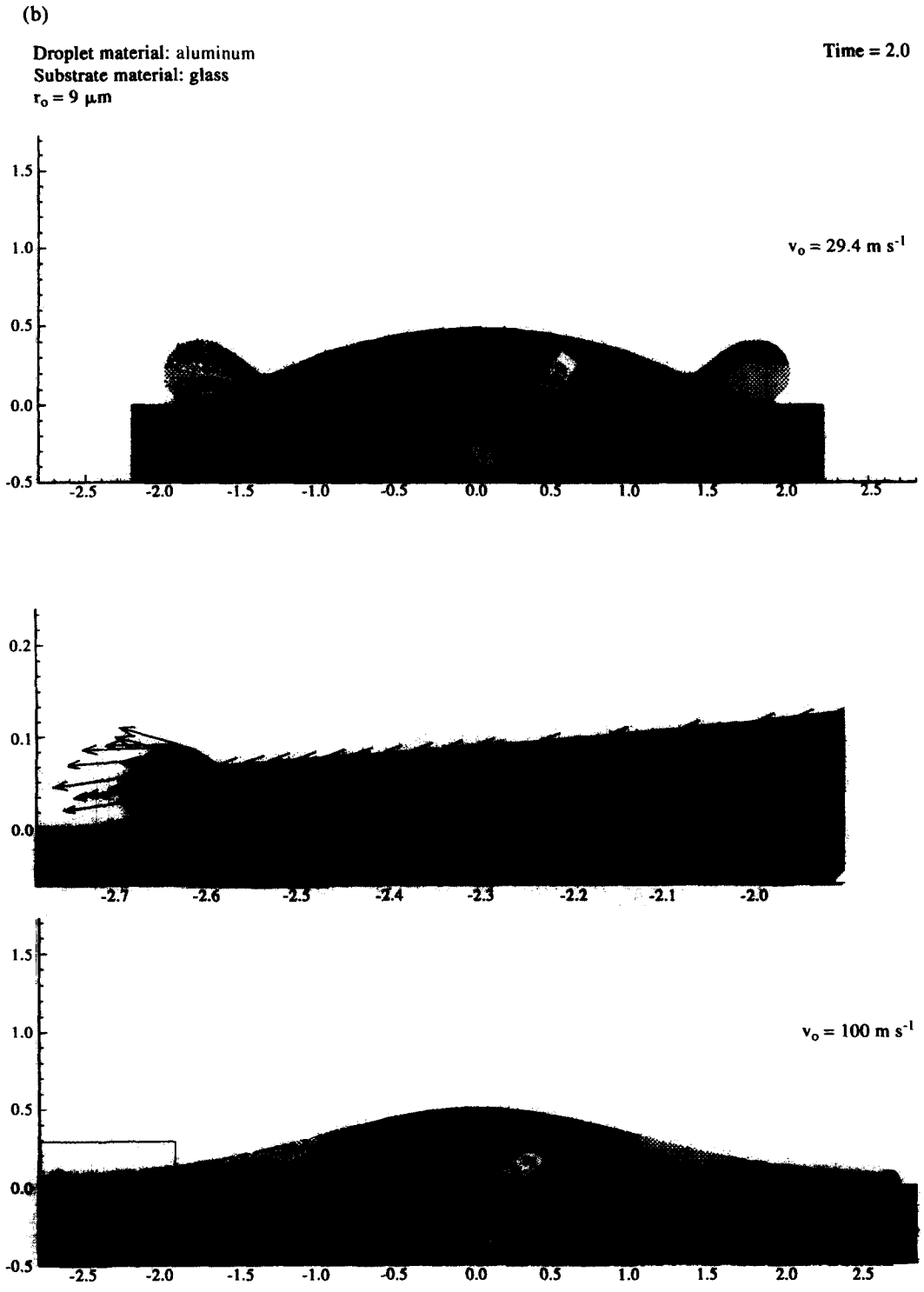

Fig. 5—*continued.*

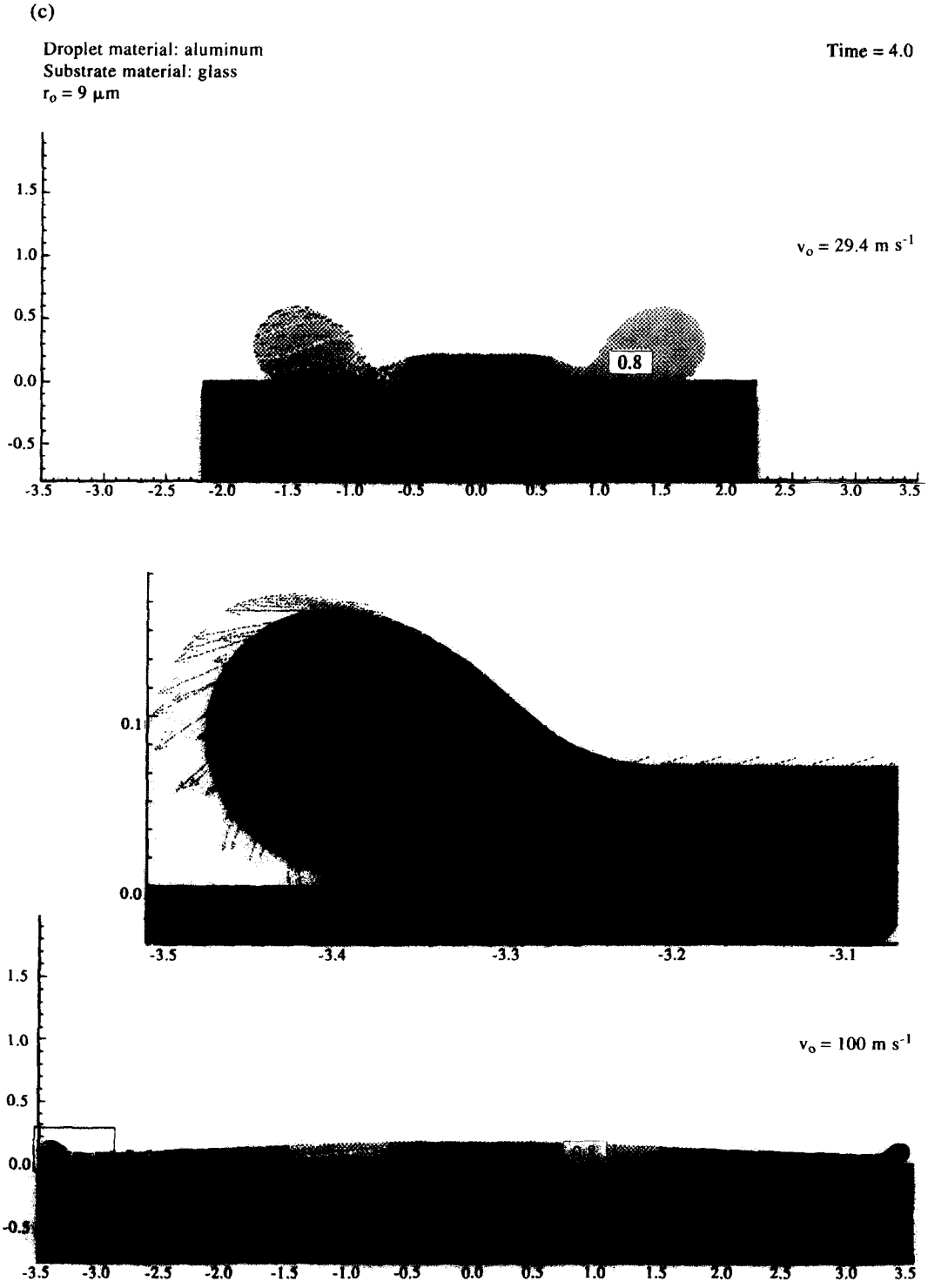

Fig. 5—*continued.*

the fluid dynamics standpoint, the droplet does not spread as much because the impact velocity is much smaller than that of Fig. 3. This facilitates the termination of the spreading process by surface tension forces. The mass accumulation around the droplet periphery is rather remarkable (Fig 4b,c). Recoiling of the droplet is in progress in Fig. 4c where the splat features a doughnut shape.

Effect of impact velocity on the cooling of a liquid metal droplet

The effect of droplet impact velocity on the spreading and cooling molten metal droplets was investigated by performing a combination of simulations for aluminum droplets. A molten aluminum droplet was chosen in our simulations because of its relevance in the thermal spray deposition process. The following physical property values were used for the molten aluminum droplets: surface-tension coefficient $\gamma = 0.914\ \mathrm{N\,m^{-1}}$, density $\rho = 2385\ \mathrm{kg\,m^{-3}}$, kinematic viscosity $\nu = 5.45 \times 10^{-7}\ \mathrm{m^2\,s^{-1}}$, thermal diffusivity $\alpha = 3.65 \times 10^{-5}\ \mathrm{m^2\,s^{-1}}$, and thermal conductivity $k = 94.03\ \mathrm{W\,m^{-1}\cdot K^{-1}}$. The substrate material was glass. The following two cases were simulated: an aluminum droplet of radius $r_0 = 9\ \mu\mathrm{m}$ impinging on a glass substrate with a velocity $v_0 = 29.4\ \mathrm{m\,s^{-1}}$ and, next, with a velocity $v_0 = 100\ \mathrm{m\,s^{-1}}$. The above conditions resulted in the following values of the relevant dimensionless numbers: $Re = 485$, $We = 20$, and $Fr = 10^7$ for the droplet impacting with $v_0 = 29.4\ \mathrm{m\,s^{-1}}$ and $Re = 1650$, $We = 235$, and $Fr = 10^8$ for the droplet impacting with $v_0 = 100\ \mathrm{m\,s^{-1}}$

The splashing and quenching sequences of the molten aluminum droplets shown in Fig. 5a–c reveal that even for a non-conductive substrate, the time scales for the fluid dynamics and heat transfer processes are comparable, especially in the high impact velocity case. This finding is in agreement with the predictions of Trapaga and Szekely [17], who concluded that cooling and spreading take place at comparable rates under a high value of heat-transfer coefficient conditions. An examination of the temperature contours in Fig 5a–c also reveals that the cooling rate is much higher at the splat outer edge than at the center region, particularly so in the case of the high impact velocity. This is because hot, molten metal is continuously supplied to the central region of the splat during the impaction process. At the spreading front of the splat, the fluid contacts the cold substrate surface continuously and it is cooled down effectively. Increasing the droplet impact velocity clearly increases the heat transfer from the droplet to the substrate. The flow details in Fig 6a–c illustrates the outward spreading velocity at the splat periphery. Mass accumulation around the splat periphery is more severe in the case of the lower velocity where recoiling also occurs faster.

Figure 6 shows quantitative evidence on the effect of droplet impact velocity and diameter on the maximum splat radius. Generally, increasing the impact velocity and droplet diameter facilitates the spreading process and yields larger diameter splats. Under identical conditions, the tin droplet spreads quite a bit more than the aluminum droplet which features a higher surface tension coefficient. To this end, the maximum value of R_{max} for the tin droplet is 1.5 times larger than the corresponding value for the aluminum droplet. In all cases shown in Fig. 6 droplet recoiling is apparent.

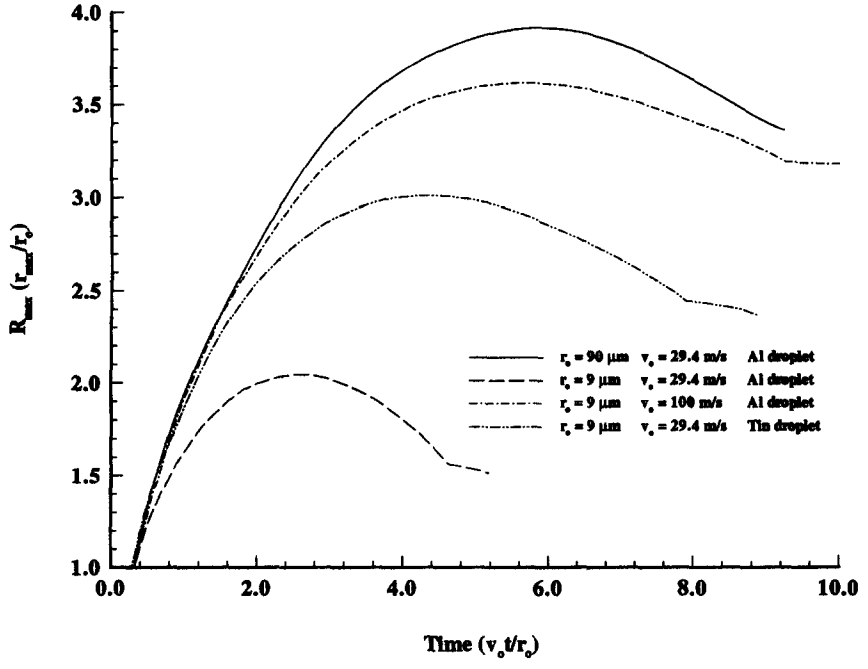

Fig. 6. Variation of maximum splat diameter with time.

5. CONCLUSIONS

This paper presented a theoretical study of the pre-solidification heat transfer of molten metal droplets impinging upon a substrate. Cooling of a hot surface with a water droplet was also considered. The theoretical model accounted for a host of phenomena, including surface tension and was solved numerically utilizing the finite element method with a deforming mesh and grid generation.

The results documented the effects of substrate thermophysical properties, impact velocity, and droplet diameter on the heat transfer and fluid dynamics of the deforming droplet. The occurrence of droplet recoiling and mass accumulation around the splat periphery were definitive features of the flow field and yielded a nonmonotonic dependence of the maximum splat radius on time. The maximum splat thickness did not always occur at the axis of symmetry. At late times it usually occurred at the periphery of the splat, where mass accumulation was observed. The droplet spreading was retarded and finally halted by the action of the surface tension and viscosity. Subsequently, flow reversal (recoiling) set in and the main flow was directed toward the axis of symmetry.

The predicted temperature distribution in a molten metal droplet during the quench cooling process exhibits strong two-dimensional features. This result suggests that a simplified one-dimensional axial conduction treatment of this process may not be always appropriate. The present study proved that at conditions near maximum spreading for high impact velocities, the heat transfer occurs mainly in the radial direction, despite the fact that the splat diameter is many times larger than the splat thickness. The numerical model predicted that the heat transfer time scales were comparable to the droplet deformation time scales. The calculated temperature distribution within a molten metal droplet revealed that the fluid temperature at the spreading front is substantially lower than the temperature at the splat center. Solidification, therefore, is expected to initiate in this case around the periphery of a deforming molten metal droplet in the neighborhood of the contact line and advance towards the splat center.

Acknowledgements—This work was partially supported by NCSA under Grant numbers CEE930000N and RCD910000N and utilized the CRAY Y-MP4/464 of the Center at the University of Illinois at Urbana-Champaign.

REFERENCES

1. A. M. Worthington, On the forms assumed by drops of liquids falling vertically on a horizontal plate, *Proc. R. Soc. Lond.* **25,** 261–271 (1877).
2. A. M. Worthington, A second paper on the forms assumed by drops of liquids falling vertically on a horizontal plate, *Proc. R. Soc. Lond.* **25,** 498–503 (1877).
3. D. J. Hayes, D. B. Wallace and M. T. Boldman, Picolite solder droplet dispension, *Proceedings ISHM*, pp. 316–321 (1992).
4. L. O'Connor, Ultralow-density alloys, *Mech. Engng ASME* **116,** 61 (1994)
5. H. Jones, *Rapid Solidification of Metals and Alloys, Monograph* 8. The Institution of Metallurgists, London (1982).
6. J. Szekely, Can advanced technology save the U. S. steel industry?, *Sci. Am.* **257,** 34–41 (1987).
7. D. Poulikakos and J. Waldvogel, Heat transfer and fluid dynamics in the process of spray deposition. In *Advances in Heat Transfer*, Vol. 28, pp. 1–73. Academic Press, San Diego (1996).
8. S. Annavarapu, D. Apelian and A. Lawley, Spray casting of steel strip: process analysis, *Metal. Trans.* **21A,** 3237–3256 (1990)
9. T. Bennett and D. Poulikakos, Splat-quench solidification: estimating the maximum spreading of a droplet impacting a solid surface, *J. Mater. Sci.* **28,** 963–970 (1993).
10. H. Jones, Cooling, freezing and substrate impact of droplets formed by rotary atomization, *J. Phys. D: Appl. Phys.* **4,** 1657–1660 (1971).
11. F. H. Harlow and J. P. Shannon, The splash of a liquid droplet, *J. Appl. Phys.* **38,** 3855–3866 (1967)
12. F. H. Harlow and J. E. W. Welch, Numerical calculation of time-dependent viscous incompressible flow of fluid with free surface, *Phys. Fluids*, **8,** 2182–2189 (1965).
13. C. S. Frederiksen and A. M. Watts, Finite element method for time-dependent incompressible free surface flow, *J. Comput. Phys.* **39,** 282–304 (1981)
14. E. A. J. Fletcher, *Computational Fluid Dynamics* Vol. II, pp. 333–345. Springer, Berlin (1988).
15. J. Madejski, Solidification of droplets on a cold surface, *Int. J. Heat Mass Transfer* **19,** 1009–1013 (1976).
16. J. Madejski, Droplets on impact with a solid surface, *Int. J. Heat Mass Transfer* **26,** 1095–1098 (1983).
17. G. Trapaga and J. Szekely, Mathematical modeling of the isothermal impingement of liquid droplets in spray processes, *Metall. Trans.* B **22,** 901–914 (1991).
18. Flow-3D, Report no. FSI-88-00-1, Flow Science Inc., Los Alamos, NM, Vols. 1–4 (1988).
19. C. W. Hirt and B. D. Nichols, Volume of fluid (VOF) method for the dynamics of free boundaries, *J. Comput. Phys.* **39,** 201 (1981).
20. K. Tsurutani, M. Yao, J. Senda and H. Fujimoto, Numerical analysis of the deformation process of a droplet impinging upon a wall, *JSME Int. J.* II **33,** 555–561 (1990).
21. T. Watanabe, I. Kuribayashi, T. Honda and A. Kanzawa, Deformation and solidification of droplet on a cold substrate. *Chem. Engng Sci.* **47,** 3059–3065 (1992).
22. M. Pasandideh-Ford and J. Mostaghimi. Deformation and solidification of molten particles on a substrate in thermal plasma spraying, *Proceedings of the 7th National Thermal Spray Conference*, pp. 405–414 (1994).
23. J. Fukai, Z. Zhao, D, Poulikakos, C. Megaridis and O. Miyatake, Modeling of the deformation of a liquid droplet impinging upon a flat surface, *Phys. Fluids* A **5,** 2588–2599 (1993).
24. P. Bach and O. Hassager, An algorithm for the use of the Lagrangian specification in Newtonian fluid mechanics and application to free-surface flow, *J. Fluid Mech.* **152,** 173–190 (1985).
25. Z. Zhao, Transport phenomena during the impingement of liquid-metal droplets on a substrate, Ph.D. Thesis, University of Illinois at Chicago (1994).
26. O. C. Zienkiewicz and R. L. Taylor, *The Finite Element Method* (4th Edn) Vol 2. pp. 513–514 McGraw-Hill, London (1991).
27. C. W. Hirt and B. D. Nichols, Adding limited compressibility to incompressible hydrocodes, *J. Comput. Phys.* **34,** 390–400 (1980).

28. M. Kawahara and H. Hirano, A finite element method for high Reynolds number viscous fluid flow using two step explicit scheme, *Int. J. Numer. Meth. Fluids* **3,** 137–163 (1983).
29. D. Poulikakos, *Heat Conduction*. Prentice Hall, Englewood Cliffs, NJ. (1994).
30. R. J. Collins, Bandwidth reduction by automatic renumbering, *Int. J. Numer. Meth. Engng* **6,** 345–356 (1973).
31. P. J. Haley and M. J. Miksis, The effect of the contact line on droplet spreading, *J. Fluid Mech.* **223,** 57–81 (1991).
32. E. Huh and L. E. Scriven, Hydrodynamic model of steady movement of a solid/liquid/fluid contact line, *J. Colloid Interface Sci.* **35,** 85–101 (1971).
33. V. E. B. Dussan and S. H. Davis, On the motion of a fluid-fluid interface along a solid surface, *J. Fluid Mech.* **65,** 71–95 (1974).
34. V. E. B. Dussan, On the spreading of liquids on solid surfaces: static and dynamic contact lines, *Ann. Rev. Fluid Mech.* **11,** 371–400 (1979).
35. W. J. Silliman and L. E. Scriven, Separating flow near a static contact: slip at a wall and shape of a free surface, *J. Comput. Phys.* **34,** 287–313 (1980).
36. L. M. Hocking and A. D. Rivers, The spreading of a drop by capillary action, *J. Fluid Mech.* **121** 425–442 (1982).
37. P. Sheng and M. Zhou, Immiscible-fluid displacement: contact-line dynamics and the velocity-depend capillary pressure, *Phys. Rev* **45,** 5694–5708 (1992).
38. L. Leger and J. F. Joanny, Liquid spreading, *Rep. Prog. Phys.* **25,** 431–486 (1992).
39. J. Fukai, Y. Shiiba, T. Yamamoto, O. Miyatake, D. Poulikakos, C. M. Megaridis, and Z. Zhao, Wetting effects on the spreading of a liquid droplet colliding with a flat surface: experiment and modeling, *Phys. Fluids* **7,** 236–247 (1995)